Energy Equip. Sys./ Vol. 13/No. 4/December 2025/ 403-414

ENERGY EQUIPSYS

Energy Equipment and Systems

www.energyequipsys.com

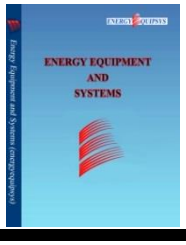

Impact driving-induced stress amplification due to flange waviness in offshore wind turbine monopile foundations

Manuscript Type

Research Paper

Authors

Mehdi Shirani*

Research Institute for Subsea Science and Technology, Isfahan University of Technology, 8415683111, Isfahan, Iran

Article history:
Received: 23 February 2025
Revised: 8 July 2025
Accepted : 3 August 2025

ABSTRACT

Impact pile driving is the preferred installation method for offshore wind monopile (MP) foundations. Due to the flange waviness, the MP wall stresses below the waviness apexes are larger during impact pile driving than in other areas. In recent designs of 3XL TP-Less monopiles, the door hole is relocated from the tower to the MP, positioned close to the flange, and the boat landing platform is eliminated. This required the door opening stiffeners and other MP internal attachments to be welded close to the flange. It is generally recommended to avoid positioning the MP wall openings and attachments in the highly stressed areas created by the flange waviness. This study aims to calculate the waviness effects on the MP wall stresses of a 3XL MP and to determine the distance from the flange at which this waviness effect disappears. Pile driving is simulated using the finite element software LS-DYNA, and flange waviness is modelled. It was found that for the studied 3XL MP weighing 2160 tons, at 60 mm below the flange, the MP wall Von Mises stress is 253 MPa at the waviness apex and 140 MPa at the waviness valley, representing an 80% increase. The flange waviness effect on the MP wall stresses gradually decreases as one moves away from the flange and diminishes 2600 mm below the flange.

Keywords: 3XL MP, TP-Less Design, Impact Driving, Flatness Tolerance, Flange Waviness, Fatigue, LS-DYNA.

1. Introduction

As a result of the innovations implemented over the last decade, offshore wind energy is becoming increasingly cost-effective. The foundation is one of the sources of cost for a wind farm. The most common foundation type for offshore wind turbines is the steel monopile (MP). Early designs used grouted connections to connect the transition piece (TP) to the MP. An attempt is being made to replace the grouted connection between the MP and TP with a bolted flange. Recent 3XL MP designs have incorporated TP-Less connections by eliminating the transition piece and directly bolting the MP to the tower [1]. Figure 1 illustrates the recent TP-Less MP installed at Germany's offshore wind farms. As shown in Fig. 1, in addition to removing the TP, the door hole is relocated from the tower to the MP, and the boat landing platform is eliminated to reduce foundation costs. Service technicians and crew can directly enter the MP and tower using motion-compensated Walk-to-Work vessels, eliminating the need for a boat landing platform —a further step in reducing offshore wind

* Corresponding author: Mehdi Shirani
Research Institute for Subsea Science and Technology, Isfahan University of Technology, 8415683111, Isfahan, Iran
Email: mehdi.shirani@iut.ac.ir

foundation costs. Eliminating the boat landing and relocating the door close to the MP flange necessitated welding the door hole stiffeners and other MP internal attachments near the flange.

In TP-Less configurations, the MP is driven into the soil, and attachments such as a ladder and internal platform are attached. To install these attachments easily, supports are welded to the MP wall during the MP fabrication process. After pile driving, the attachments are easily connected to the MP using these welded supports. Eliminating the grouted connection and, recently, TP, and using a bolted connection implies that the pile-driving operation, using a hydraulic hammer, is directly performed on the flange surface. Figure 2 shows a schematic of the pile-driving process using an impact hammer.

When the monopile is transported to the site, it is upended and driven into the seabed using an impact hammer. A movable ram section is repeatedly dropped onto an anvil, which transfers the kinetic energy into the pile, driving it through the seabed. A Hydro hammer can be seen in Fig. 3.

Fig. 1. TP-Less MP at German offshore wind projects [2]

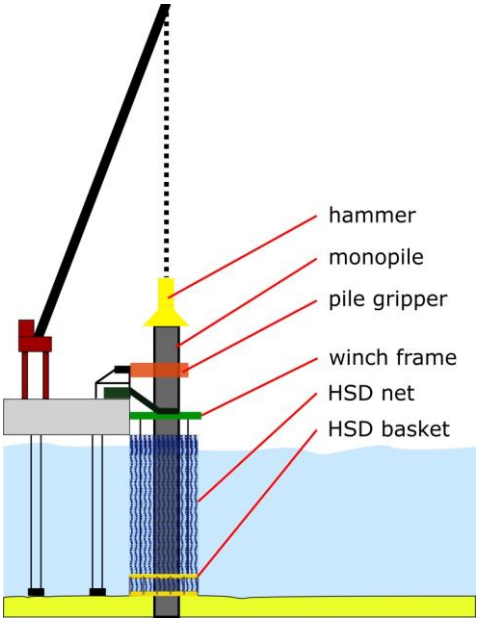

Fig. 2. Pile-driving by an impact hammer [3]

Fig. 3. An IHS S-4000 Hydro hammer [4]

When the anvil ring impacts the flange, an elastic wave is created and propagated in the MP axial direction [5]. The MP wall and attachments vibrate when the elastic wave passes through the MP. This vibration causes large fluctuations and fatigue damage to the MP wall welded connections and attachments welded to the MP. Since the hammer and MP are axisymmetric, the created elastic wave is expected to be axisymmetric. However, this is not true due to the flange fabrication tolerances. One of these is flange flatness tolerance or waviness. Fig. 4 shows an exaggerated view of flange waviness.

Due to this waviness, the created elastic wave is not axisymmetric. In reality, the anvil ring contacts the MP on the apexes of these waves. Therefore, the attachments welded below the waviness apex, close to the MP flange, are subjected to larger stresses and much larger fatigue damage. This waviness effect on the MP wall stresses disappears at some distances from the MP flange.

This study aims to determine the distance from the MP flange at which this effect vanishes. This is important to know, as in the initial stage of the MP design, the designer needs to locate the positions of the support attachments and MP openings. It is better to avoid positioning the attachments in an area heavily affected by flange waviness. Few studies on pile-driving flange stress analysis have been published [6, 7]. To the author's knowledge, no one considers flange manufacturing tolerances, particularly the impact of flange waviness on the MP wall stress during pile driving. Most published studies focus on the in-place ULS and FLS design of monopile flange-welded connections, as well as the effects of imperfections [8, 9].

This study aims to evaluate the influence of flange waviness on 3XL MP wall stresses during pile driving. To achieve this goal, an ANSYS LS-DYNA finite element model of the hammer and MP is created [10], and the pile driving analysis is modelled. The flange waviness is modelled, and the MP wall stresses are plotted at different distances from the MP.

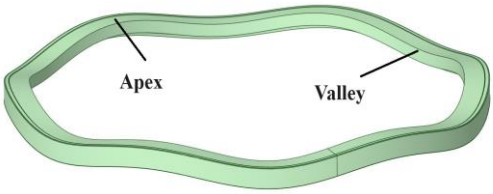

Fig. 4. Exaggerated view of flange waviness

The following sections introduce the MP and flange geometry, material, hammer, boundary condition, simulation parameters, mesh, contact, and results.

This study contributes to a deeper understanding of the mechanical behaviour of offshore wind energy support structures during the installation phase. By analysing the influence of flange manufacturing tolerances on stress distribution during impact pile driving, the findings provide valuable insights into the reliability, safety, and performance optimisation of critical energy infrastructure components—areas that align closely with the scope of Energy Equipment and Systems.

2. Finite element model

The finite element model is built using ANSYS Workbench LS-DYNA. Solid elements are used to model the hammer and flange, and shell elements are used to model the MP wall.

2.1. Geometry

Figure 5 shows the pile driving model setup. Figure 6 shows the MP geometry. The MP weight is 2160 tons. Figure 7 shows the cross-section of an MP flange.

The flange's outer diameter is 8000 mm, and the inner diameter is 7200 mm. Figure 7 shows the cross-section of an MP flange. An essential characteristic of flanges that withstand pile-driving loads is their inclination towards the inside. Gap g ensures that the loads act only within the horizontal contact area c [11]. Here, c is 50 mm, g is 0.9 degrees, a is 35 mm, and b is 70 mm.

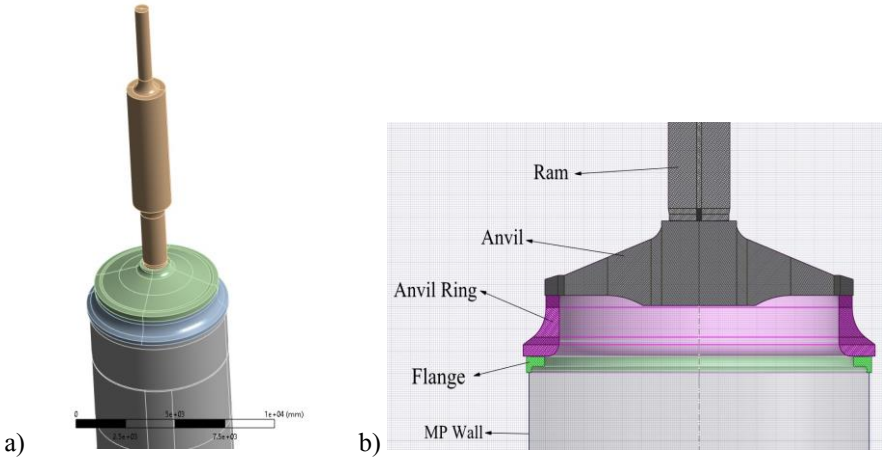

Fig. 5. Pile driving model set-up

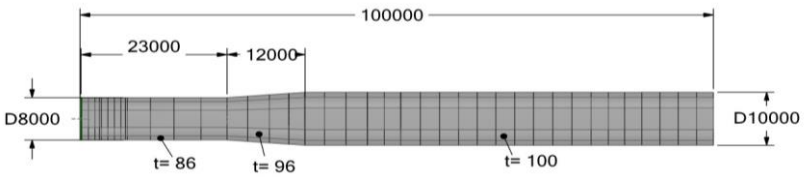

Fig. 6. In the MP geometry, all dimensions are in mm

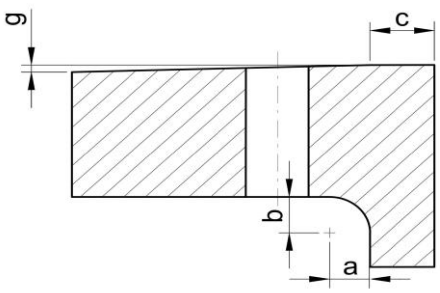

Fig. 7. Typical MP Flange cross-section

2.2. Flange flatness tolerance, waviness

There has been considerable debate regarding the waviness tolerances for flange bolted connections in wind turbine support structures [12]. Ref. [13] provides a historical overview of these tolerance requirements. Ref. [14] and [15] suggest a tolerance of 2.0 mm for flange waviness across the entire circumference. The values were derived from industry experience. In this study, the out-of-flatness of the flange surface for MP and TP is modelled using 6 × 60-degree sinusoidal waves of amplitude 1 *mm*. The out-of-flatness modelling is represented in Fig. 8.

2.3. Material

The MP and hammer are constructed of structural steel with Young's Modulus of 2.1E5 MPa, Poisson's Ratio of 0.3, and density of 7850 $\frac{kg}{m^3}$.

2.4. Hammer

A hydro hammer, with a strike power of 4000 *kJ* and a ram weight of 200 tons, is used for pile driving, Fig. 3.

2.4.1. Hammer Impact

During the pile driving process, the ram is lifted to a certain height during driving and then released. It freely drops onto the anvil, transferring the load to the monopile. The potential energy is converted into kinetic energy, inducing a force pulse that propagates through the monopile. Modelling the free fall of the anvil isn't essential for MP integrity analysis. The impact load is transferred from the ram to the anvil when the ram makes contact with the anvil. Therefore, the most critical parameter is the speed at which the ram impacts the anvil. During this impact, energy is given to the anvil and, subsequently, the flange. In the FE model, the ram is in contact with the anvil, the anvil is in contact with the anvil ring, and the anvil ring is in contact with the flange. This study uses a 4000-*kJ* hammer. By neglecting the hammer losses, the energy, *E*, given to the anvil by the ram should be 3230 *kJ*; therefore, the ram speed, *V*, can be calculated. Ram weight, *M*, is 200 tons; therefore, the ram speed in contact with the anvil is:

$$E = \frac{1}{2} \times MV^2 \quad \Rightarrow V = \sqrt{\frac{2 \times E}{M}} = 5.66 \frac{m}{s} \tag{1}$$

2.5. Boundary condition

During pile driving, the compressive stress wave induced by the impact between the ram and anvil travels downward through the pile. The magnitude of the compressive stress wave gradually decreases due to the losses between the MP wall and water and between the MP wall and soil. When the compressive stress wave reaches the pile tip, it reflects and moves upward again [16]. As can be seen in section 2.9, the flange waviness effect on the MP wall stresses diminishes before the stress wave reaches the conical section of the MP. Therefore, the reflected wave from the MP tip is not interesting to this study. The MP is assumed to be free-ended, and no boundary condition is applied to the MP tip. Fig. 9 shows the general set-up of the FE model and boundary conditions.

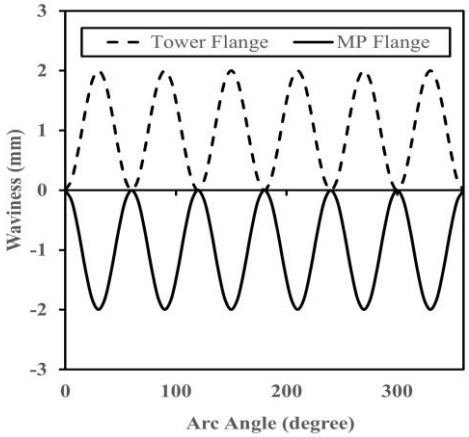

Fig. 8. Flange Waviness

Fig. 9. General set-up of the FE model and boundary conditions

2.6. Simulation time

3D dynamic modelling of the pile driving process is computationally expensive and time-consuming. This simulation aims to find the distance below the flange at which stresses are affected by the flange waviness. Due to this, only the time required for the elastic wave to travel between the flange and the MP tip is simulated. Elastic waves in steel have a speed of c equal to:

$$c = \sqrt{\frac{E}{\rho}} = 5172 \frac{m}{s} \quad (2)$$

where E represents Young's Modulus and ρ represents the steel density, as given in Section 2.3.

Since the MP length is 100 meters, the simulation time of 100/5172 = 0.019 s is enough for this study. The driving process is modelled for 0.022 s.

According to Ref. [17], the critical time step is:

$$\triangle t_{min} = \frac{l}{c} \quad (3)$$

where l represents the smallest element size and c represents the wave speed in steel. If the simulation time step exceeds the critical time step, the simulation error will be significant and unacceptable. More accurate results can be obtained if the simulation time step is smaller than the critical time step, but the simulation time will increase substantially. LS-DYNA can determine the critical time step for the analysis based on the mesh size and wave speed in steel. Figure 10a provides a summary of the calculated critical time step for solid parts of the model, and Fig. 10 b provides a summary of the calculated critical time step for shell parts. The calculated minimum critical time step for solid parts is 6.17 × 10^ (-7) s, and for the shell part, it is 2.05 × 10^ (-6) s. This study employs a simulation time step of 2 × 10^-7 s.

2.7. Mesh

The hammer and flange are modelled using solid elements, while the MP wall uses shell elements. Modelling the MP wall using solid aspects resulted in many elements, making it extremely time-consuming to run the problem. Therefore, shell elements are used for the MP wall. Figure 11 shows the mesh used in this study. The LS-DYNA fully integrated S/R (Selective Reduced) solid element (ELFORM 2) is used to model the solid parts of the model. The LS-DYNA fully integrated shell element (ELFORM 16) models the MP wall. The anvil, anvil ring, and flange mesh size is 30 mm. The MP wall mesh size is 120 mm.

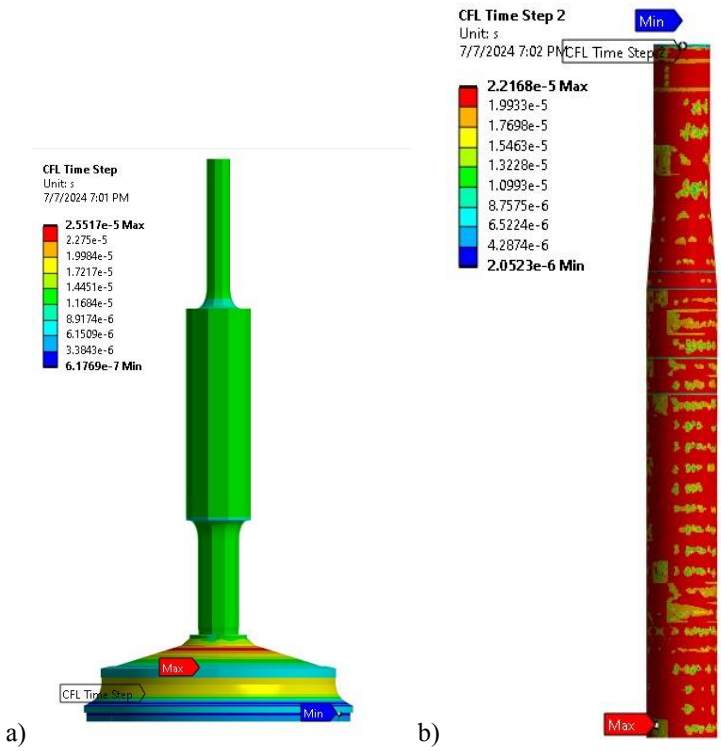

a) b)

Fig. 10. Calculated critical time step: a) solid parts of the model, b) shell parts

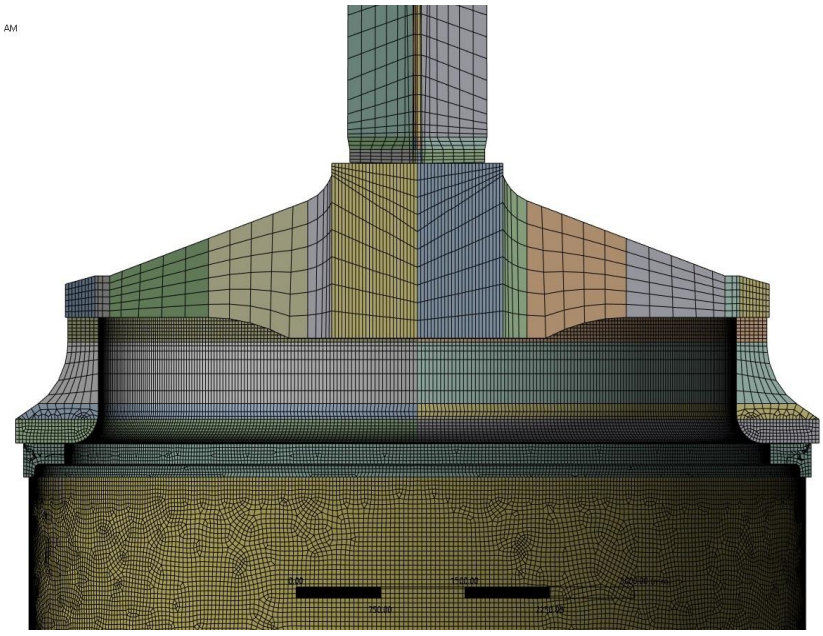

Fig. 11. Model mesh

2.8. Contact

A frictional contact with a friction coefficient of 0.2 is used to model the contact between the ram and anvil, the anvil and anvil ring, and the anvil ring and flange.

2.9. Results

2.9.1. Energy Summary

The system's total energy should always be conserved in explicit dynamic simulations to obtain accurate results. To validate the analysis

performed with LS-DYNA, the system's total energy should be constant during the analysis and equal to the initial total energy. Figure 12 shows the energy balance diagram. As can be seen, the system's total energy is constant and equal to the initial hammer energy of 3230 kJ. According to the LS-DYNA manual, the total energy is the sum of kinetic, internal, contact (sliding), system damping, hourglass and rigid wall energy. As mentioned in section 2.5, the soil is not modelled, and the model is free-ended. Also, no material damping is considered in the model. Therefore, the system damping energy is zero. Rigid wall energy is also zero. The hourglass energy is zero, indicating that there is no hourglass deformation in the model. In LS-DYNA, sliding energy is dissipated from sliding between contacting surfaces in a finite element simulation. Here, the sliding energy is 86 kJ, 2.7% of the system's total energy. Fig. 13 illustrates the transfer of energy from the ram to the anvil, anvil ring, and MP. According to Fig. 13, at t = 0.02 s, the ram energy is 84 kJ, the anvil energy is 32 kJ, the anvil ring energy is 18 kJ, and the MP energy is 3010 kJ. Additionally, according to Fig. 12, the sliding energy is 88 kJ, and the sum of these energies is 3,230 kJ, which is equal to the initial ram energy given to the system.

2.9.2. Contact

To ensure that the contacts behave as expected and penetration is within acceptable values, the maximum and minimum values of the nodal contact gap for each node on the contact surfaces during the analysis time are plotted in Fig. 14a and b. The figures illustrate the contact areas between the ram and anvil, the anvil and anvil ring, and the flange. As can be seen, both plots show the maximum value of the contact gap over time for node 36525 and the minimum value for node 25074. Both nodes belong to the contact surface between the ram and anvil. Fig. 15 shows the time history of the contact gap for these two nodes. The negative value represents the maximum contact penetration of -1.5 mm. This contact penetration is due to the large mesh on the ram's contact with the anvil. Using the finer mesh, the penetration will approach much lower values.

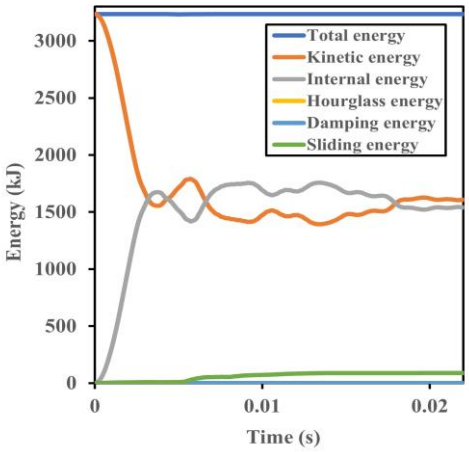

Fig. 12. Energy balance

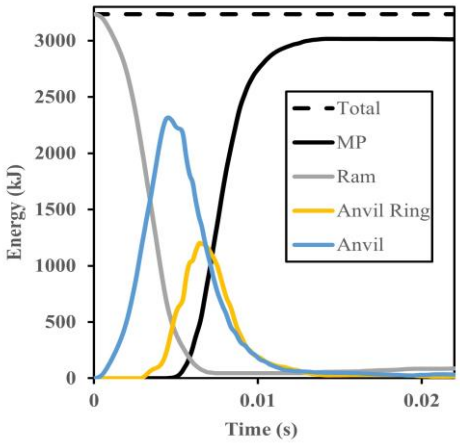

Fig. 13. Energy transfer from the ram to the MP

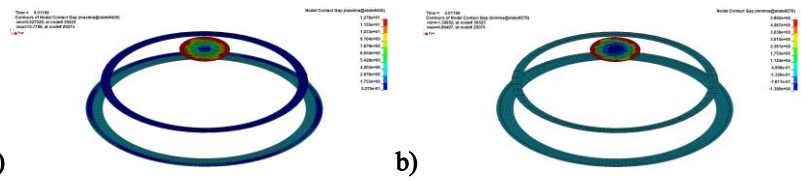

Fig. 14. Nodal contact gap a) Maximum value for each node over the analysis time, b) minimum value

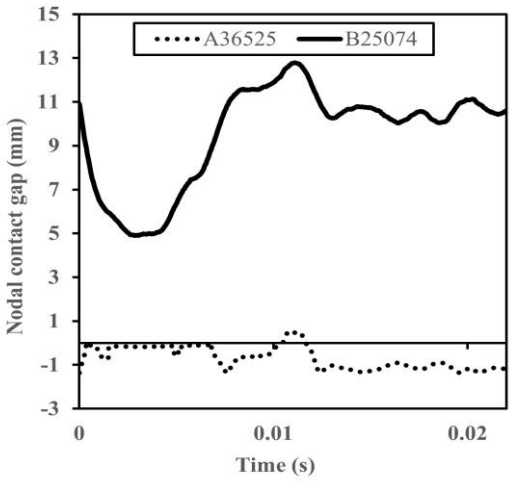

Fig. 15. Time history of the contact gap for nodes 36525 and 25074

2.9.3. Stress wave

When the ram hits the anvil, a compressive stress wave that travels along the MP is induced. The compressive wave speed is calculated in section 2.6 and equals 5172 m/s. Due to the flange waviness (Fig. 8), the anvil ring contacts the MP flange at the six apexes. Fig. 16 shows the vector plot of the flange contact force at t = 0.0067 s when the flange contact force peaks. Figure 17 shows the MP wall Von Mises stress at t = 0.0067 s while the compressive stress wave passes along the MP. As can be seen, the areas below the flange waviness apex experience larger stresses than the areas below the flange waviness valley. To evaluate how the stresses below the flange apex and valley change by moving away from the flange, two-element paths are defined and presented in Fig. 18: one below the flange apex and one below the flange valley. Figure 19 shows the Von Mises stress plot for MP wall elements with different distances below the flange apex and valley along the defined paths. For the presented plots in Figs. 19a, b, c, and d, the maximum stress occurs at t = 0.00844 s, 0.00847 s, 0.00759 s, and 0.00775 s, respectively. Fig. 20 plots the MP wall Von Mises stress at different times corresponding to stress peaks in Fig. 19. Figure 21 plots the difference between the Von Mises stress below the apex and valley to varying distances below the MP along the defined paths when the stresses peak. As can be seen, the Von Mises stress under the apex, at 60 mm below the flange, is 113 MPa greater than that of the element with the same distance below the valley. This difference in stresses gradually decreases as one moves away from the flange, and at 2600 mm below the MP, the difference is almost negligible.

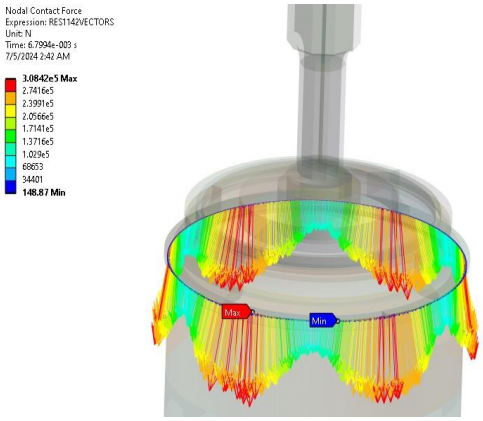

Fig. 16. Vector plot of the flange contact force at t = 0.0067 s

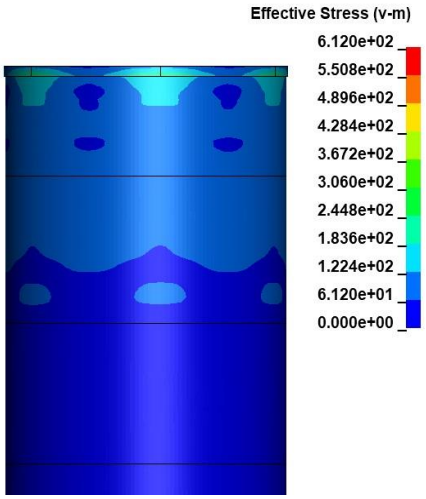

Fig. 17. MP wall Von Mises stress at t = 0.0067 s

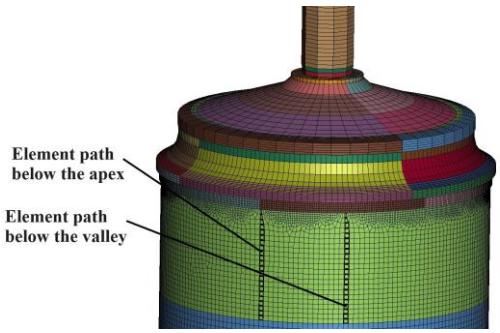

Fig. 18. Element paths below flange waviness apex and valley

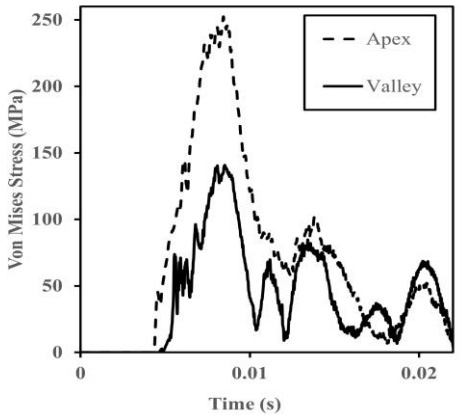

a)

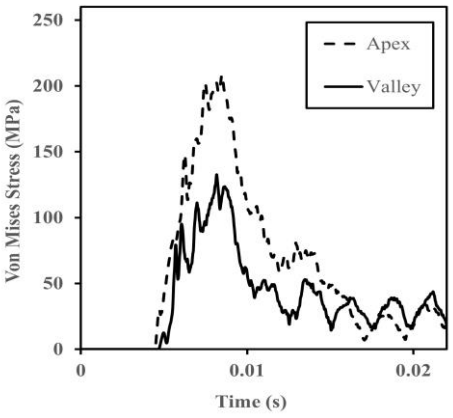

b)

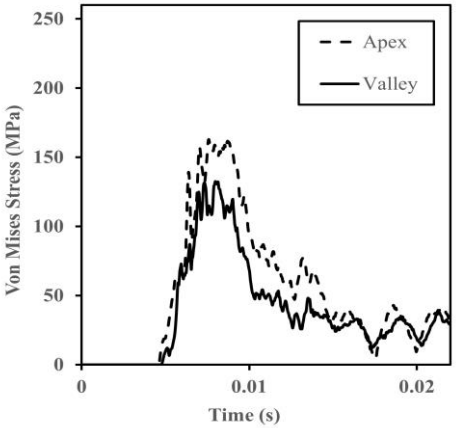

c)

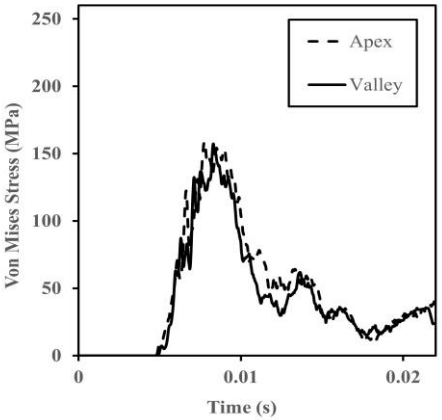

d)

Fig. 19. MP wall Von Mises stress along the paths below flange apex and valley: a) 60 mm below the flange, b) 800 mm below the flange, c) 1500 mm below the flange and d) 2600 mm below the flange

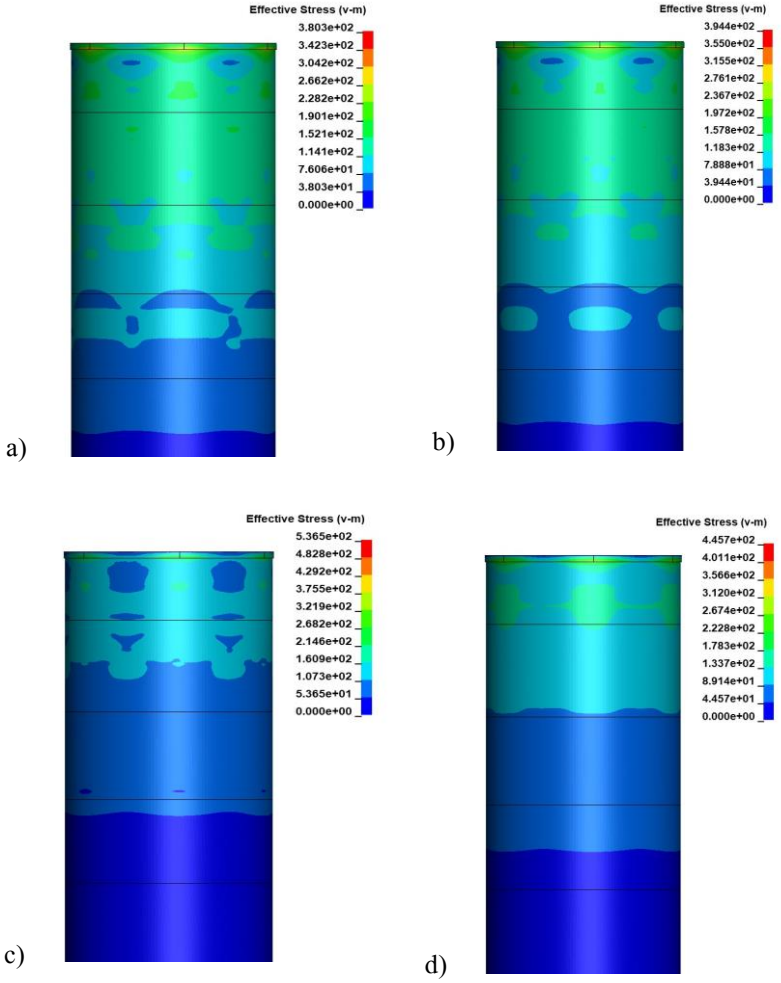

Fig. 20. MP wall Von Mises stress: a) t = 0.00844 s, b) t = 0.00847 s, c) t = 0.00759 s and d) t = 0.00775 s

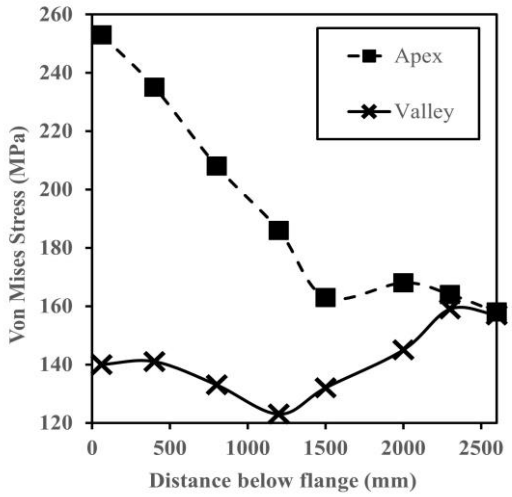

Fig. 21. Flange waviness effect on the MP wall stresses

3. Conclusion

In the recent design of TP-Less monopiles, support attachments and the door hole are placed close to the flange. One of the flange manufacturing tolerances is the flatness or waviness tolerance. Due to this waviness, during the pile driving process, areas below the flange waviness apex experience larger stresses than areas below the waviness valley. This study aims to determine the magnitude of the waviness effect on stresses below the MP flange and identify the distance at which this waviness effect is weakened or disappears. This study evaluates a 2160-ton 3XL monopile with a flange outer diameter of 8000 mm. In ANSYS LS-DYNA, a 3D finite element model is developed for the impact pile driving process of the MP, simulating the stress wave created by the hammer's impact on the flange surface. According to the available design guidelines, flange waviness is modelled using six sinusoidal waves of 1 mm amplitude. The simulation results show that at 60 mm below the flange, the MP wall's Von Mises stress is 253 MPa at the waviness apex and 140 MPa at the waviness valley. This waviness effect gradually diminishes and disappears at 2600 mm below the MP flange. A plot compares the MP wall stresses below the flange waviness and valley at different distances below the MP. Designers can use this plot to position the MP wall attachments in 3XL TP-Less MPs in the early stages of the design.

References

[1] Kurstjens M, Erents, S, Considerations when moving to tp-less. Pros and cons of tp-less monopiles ;2022.

[2] Memija A, First tp-less monopiles in place at Orsted german offshore wind projects, 2023.

[3] HSD-System, Offnoise-solutions, 2024.

[4] Offshorewind.biz, Hydrohammer s-4000 installs first monopiles, 2016.

[5] Randolph M. Analysis of the dynamics of pile driving. Advanced geotechnical analyses: CRC Press; 1991. p. 233-82.

[6] Li Y, Li J, Shi W, Li X, Wang B. Analysis of the dynamic characteristics of the top flange pile driving process of a novel monopile foundation without a transition section. Sustainability. 2022;14(10):5950.

[7] Orlando M, Ligthart J, van Wijk J, Raymackers S. PDA measurements: fact or fiction. 11th International Conference on Stress Wave Theory and Design and Testing Methods for Deep Foundations; 2022.

[8] Seidel M, Wegener F, van Dijk I. Influence of flange dimensions and geometrical imperfections on stress concentrations at welded flange necks. Stahlbau. 2020;89(11):932-43.

[9] Jorgensen J, Hodkiewicz M, Cripps E, Hassan GM, editors. An open-source analysis workflow for geometrically imperfect bolted ring-flanges in wind turbine support structures. Journal of Physics: Conference Series; 2024: IOP Publishing.

[10] K. U. MANUAL, Ls-dyna, 1992.

[11] Durstewitz M, Lange B, Schuldt L, Spriestersbach S. Document Control Sheet. 2017.

[12] Bartminn D, Griesshaber T, Lüddecke F, Al Otaibi W, Wirth R. Gerammte Ringflanschverbindungen von Monopfahlgründungen: FE-basierte Sensitivitätsanalysen im Vergleich mit Messergebnissen während der Installation. Stahlbau. 2016;85(9):591-603.

[13] Seidel M. Tolerance requirements for flange connections in wind turbine support structures. Stahlbau. 2018;87(9):880-7.

[14] Seidel M, Faber T. Zur bemessungs-und fertigungspraxis geschraubter ringflanschverbindungen bei windenergieanlagen. Deutsches Institut für Bautechnik Mitteilungen. 2008;39(3):90.

[15] Dnv G. DNVGL-ST-0126: Support structures for wind turbines. Oslo, Norway: DNV GL. 2016;632.

[16] Orlando M, Ligthart J, Wijk J. V, Schaap M, Pile installation fatigue damage from impact driving records a case study of offshore monopiles, in: Conference on Foundation Decarbonization and Re-use, Amsterdam, 2023.

[17] Ling C, Wang L, Kan C-D, Yang C. Thermal–Electrical–Mechanical Coupled Finite Element Models for Battery Electric Vehicle. Machines. 2024;12(9):596